Force and Pressure Study of Thick Cambered/Twisted 58 deg Delta Wings

Julio Chu* and John E. Lamar†
NASA Langley Research Center, Hampton, Virginia

This paper summarizes the results of a force, moment, and pressure experiment involving six thick, cambered and twisted, delta wings with 58 deg leading-edge sweep. The goal of this study was to determine a configuration that was self-trimming at a design lift coefficient of 0.25 and Mach number of 0.80. Analysis of the forces and moments data did not indicate a configuration that satisfied the design constraints; however, the configuration that came closest and had the best overall performance was selected for detailed pressure study. Wing pressure data and limited surface oil-flow photographs for this configuration showed attached flow at the design point. The associated inviscid forces and moments solutions from the Vortex Lattice Method-Suction Analogy, PAN AIR, FLO-28, and FLO-57 were compared with experimental data and showed varying levels of success. The computed pressures obtained from the PAN AIR, FLO-28, and FLO-57 for an angle of attack of 6.08 deg underpredicted the measured upper-surface pressure peak. At higher angles of attack, the lower-surface theoretical and measured pressure data compared well, whereas the upper-surface pressure predictions only approximated the trends but not the pressure level. Of the three codes, the PAN AIR is shown to be the best overall predictor.

Nomenclature

B_i	= center body camber, supercritical camber when $i = 1$, conventional camber when $i = 2$
b	= theoretical wing semispan, 16.771 in.
C_D	= total drag coefficient, drag/$q_\infty S_{\text{ref}}$
ΔC_D	= $C_D - C_{D,\min}$
C_L	= total lift coefficient, lift/$q_\infty S_{\text{ref}}$
C_m	= total pitching moment coefficient about $\bar{c}/4$, pitching moment/$q_\infty S_{\text{ref}} \bar{c}$
C_p	= pressure coefficient, $(p - p_\infty)/q_\infty$
$\bar{c}$	= mean aerodynamic chord, in.
L/D	= lift-to-drag ratio, C_L/C_D
M	= Mach number
p	= local static pressure, lbf/ft^2
p_∞, q_∞	= freestream static and dynamic pressure, respectively, lbf/ft^2
S_{ref}	= reference area projection of wing with leading edge extended to the centerline
T_j	= wingtip sets, least twist when $j = 1$, moderate twist when $j = 2$, most twist when $j = 3$
t/c	= local thickness ratio
x	= streamwise distance from local leading edge, in.
y	= local span distance measured from coordinates axes, in.
α	= angle of attack, deg
η	= $2y/b$

Subscripts

d	= design
i	= initial
max	= maximum
min	= minimum
trim	= value at trim condition

Abbreviations

FLO-28	= potential flow code
FLO-57	= Euler code
PAN AIR	= panel aerodynamics
VLM	= vortex lattice method
SA	= suction analogy

Introduction

BASED on the open literature, it is well documented that there is an increased interest in all-wing aircraft configurations for either military or commercial applications. At the cruise point, these configurations must have low drag and must also be self-trimming. Hence, the design requirements for them are more stringent than for a wing in a wing/tail or wing/canard arrangement. When the project that developed the present model was initiated in the early 1970s, there was no high-subsonic design methodology available to the Air Force contractor. Thus, the designers selected two different center bodies and used the vortex lattice method (VLM) and the Woodward's supersonic code in their analysis modes to develop three different tip twist distributions. These five components were fabricated and wind tunnel tested in all combinations to determine if one was self-trimming about the configuration $\bar{c}/4$. The design conditions were lift coefficient of 0.25 and Mach number of 0.80.

This paper summarizes the results of the high-subsonic-speed wind tunnel tests, which consisted of the force and moment test for all six body/wing tip configurations reported in Ref. 1, and a follow-on surface pressure test for the configuration that performed best at the design angles of attack and speeds. Correlations of the measured and theoretical data are presented.

Model Description and Test Conditions

The models were basically 58 deg delta wings with rounded tips and apexes. They were composed of a center body, which extended slightly beyond the theoretical midsemispan and a wing tip set. The actual sectional shapes were determined with a precision measuring instrument; the model coordinates were documented in Ref. 1. The inboard part of the model (center body) has either supercritical camber B_1 or conventional camber B_2. Figures 1 and 2 highlight the two camber types. The

Presented as Paper 86-0169 at the AIAA 24th Aerospace Sciences Meeting, Reno, NV, Jan. 6–9, 1986; received Feb. 11, 1987; revision received May 19, 1987.

*Aerospace Technologist. Member AIAA.
†Senior Research Scientist. Associate Fellow AIAA.

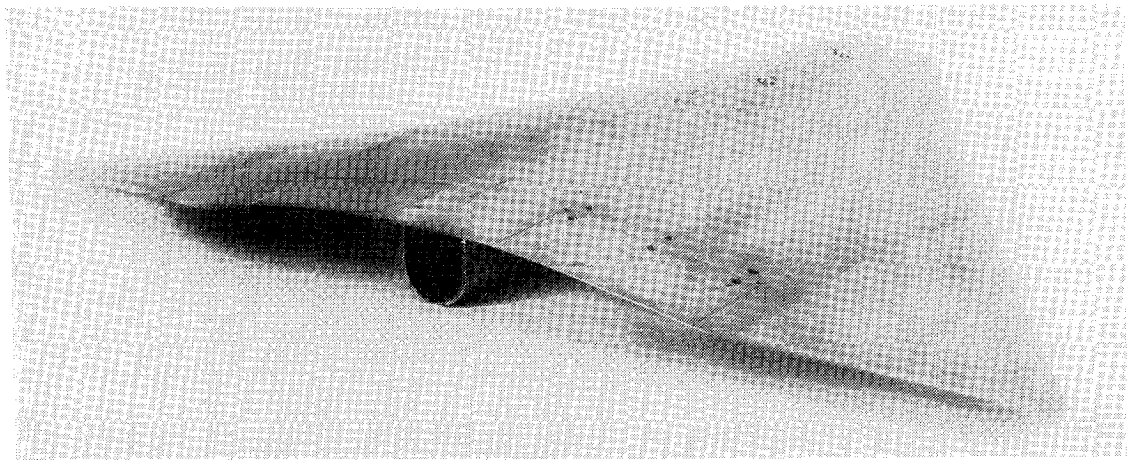

Fig. 1 Typical wing configuration: supercritical cambered center body plus wing tip set with moderate twist, $B_1 + T_2$.

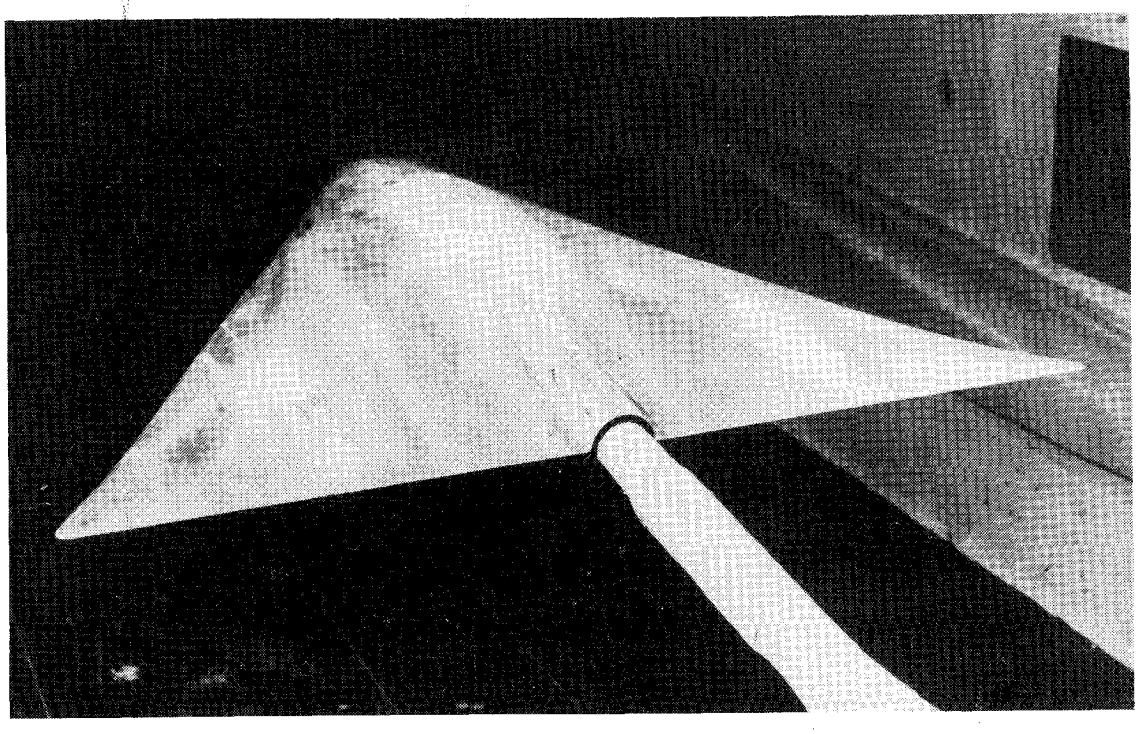

Fig. 2 Typical wing configuration: conventional cambered center body plus wing tip set with most twist, $B_1 + T_3$.

variation of maximum thickness ratio with span for these two center bodies is shown in Fig. 3, where the value of this ratio at the root is seen to be about 0.148 for B_1 and about 0.140 for B_2. The center bodies have different incidence distributions, as shown in Fig. 4. Configuration B_1 is seen to have more body twist relative to B_2; however, B_1 has a higher initial incidence than B_2. Near the theoretical midsemispan, the wing sections for both center bodies are identical to the inner portion of the wingtip sets so that they may be interchanged. The three wing tip sets T_1, T_2, and T_3 have essentially the same $(t/c)_{max}$ distribution (Fig. 3) and are distinguished by the increasing amount of twist, with set T_1 having the smallest and set T_3 the largest (Fig. 5).

The test was conducted at the NASA Langley 7 by 10 ft high-speed tunnel for Mach numbers of 0.75, 0.80, and 0.83. These Mach numbers were below, equal to, and above the design value of 0.80 and were selected to study the sensitivity of force and moment data to small changes in Mach number near M_d. For this presentation, discussions will be focused toward the $M = 0.80$ results.

Results and Discussion

Data

Force

The process of determining the best wing configuration was reported in Ref. 1, in which the effects of increasing geometrical wing tip twist (T_1 to T_3) on the wing static longitudinal stability were assessed for each center body, B_1 and B_2. As expected, of the three wing tip sets, T_3 (having the most twist) showed the highest value of trimmed lift coefficient for either body installation ($C_{L,trim} \approx 0.19$). However, these two configurations ($B_1 + T_3$ and $B_2 + T_3$) were unable to generate zero C_m at the design C_L, although this requirement may be realized with reduced static stability. The wing configuration $B_2 + T_3$ was eventually selected based on the slightly higher L/D values attained through most of the positive C_L range (Fig. 6) and the generally lower angle of attack required to achieve a given lift coefficient (Fig. 7). The latter observation is consistent with the difference between the two types of camber, where B_2 has more positive camber. Note that the total drag incurred by various

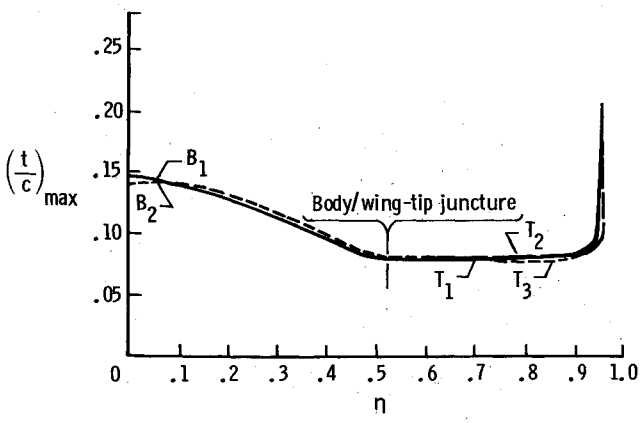

Fig. 3 Wing maximum thickness distribution.

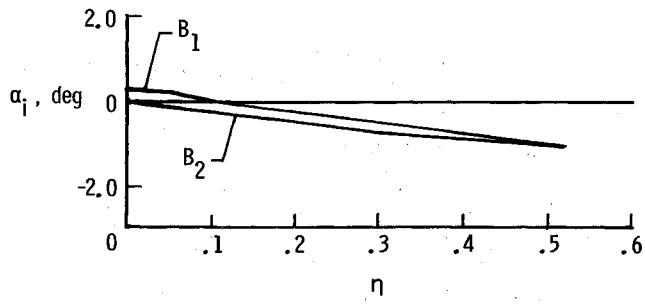

Fig. 4 Center body incidence distribution.

wing configurations near the design condition was essentially of equal magnitude.

Pressure

The purpose of the pressure investigation was to determine the extent to which attached flow was present at the design point for the selected wing. Pressure measurements for configuration $B_2 + T_3$ were recorded at nondimensional semispan stations of 0.10, 0.30, 0.60, and 0.80. The experimental data at the design conditions (associated α of 6.08 deg) are shown in Fig. 8. Examination of the pressure data indicates the presence of attached flow over the wing. In particular, a well-defined, thin-airfoil type of flow exists outboard, with typical leading-edge suction peak and smooth pressure gradients inboard. It is of interest to note that the upper- and lower-surface pressure curves cross in the trailing-edge region and that, upon integration of the pressures in this region, the resulting normal force is down. This contributes to the positive pitching moment for the self-trimming feature of the configuration. The associated surface oil-flow photograph for $\alpha = 6.07$ deg (Fig. 9) shows the global attached flow features depicted by the local pressure measurements.

Based on the pressure data and oil-flow photograph, it is apparent that the attached flow was achieved at the design point. However, it is also instructive to examine whether this flow is maintained at higher angles of attack. Inspection of the pressure measurements for nominal α of 9.7 and 13.0 deg in Fig. 10 shows that overall attached flow is present at the two inner-span stations having thicker airfoil sections. A close examination of the pressure distributions for these two stations at $\alpha = 9.7$ deg reveals that an adverse pressure gradient region exists near midchord. This indicates the presence of a recompression, but its location could not be resolved precisely because of too few pressure orifices. Also, the crossing of the

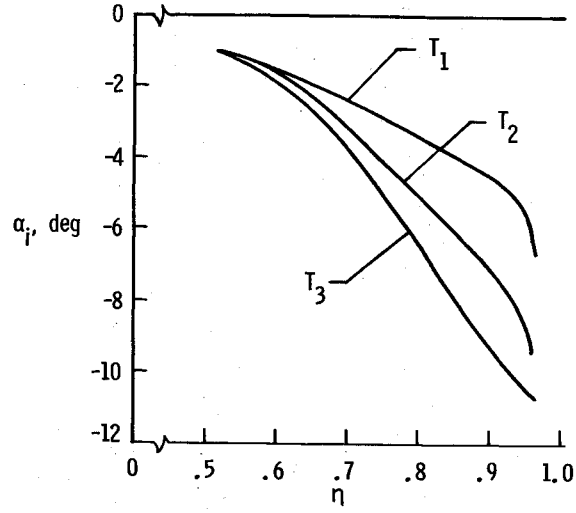

Fig. 5 Wing tip incidence distribution.

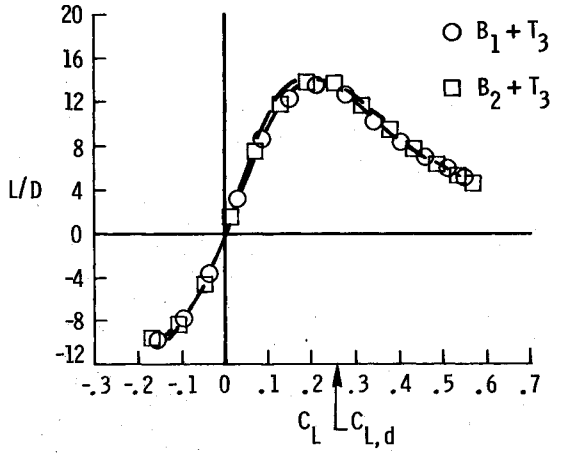

Fig. 6 Body camber effect on wing lift-to-drag ratio (wing tip set with most twist, $M_d = 0.80$).

upper- and lower-surface pressures that was observed at $\alpha = 6.08$ deg has moved aft and inboard with increasing angle of attack, resulting in a reduction of the nose-up pitching moment contribution from the trailing-edge region. Note that tip stall, caused by the loss of leading-edge suction pressures, is observed outboard and migrates inboard as the angle of attack is increased. The expanded suction envelope near midchord, shown at $\eta = 0.60$ for $\alpha = 9.70$ deg, indicates that vortex flow was developed prior to the noted tip stall.

Comparison with Theory

The computer codes employed in this study were the vortex lattice method coupled with the suction analogy (VLM-SA),[2] PAN AIR,[3] FLO-28,[4] and FLO-57.[5] The computational arrangement for each code is 168 (7 chordwise and 24 spanwise), 435 (30 chordwise and 16 spanwise), $145 \times 17 \times 33$, and $96 \times 16 \times 16$, respectively. For the VLM-SA code, solutions were obtained for angles of attack that encompassed the test angle-of-attack range whereas, for the PAN AIR and FLO-57 codes, solutions were obtained for the nominal angles of attack of 6.1, 9.7, and 13.0 deg; for the FLO-28 code, solutions for only $\alpha = 6.1$ and 9.7 deg were available.

The formulation of these employed codes is based on inviscid flow model and no boundary-layer modeling has been incorporated. All of the codes (except the VLM-SA) model the

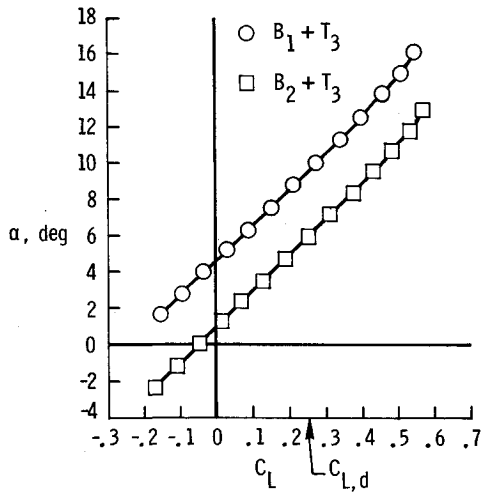

Fig. 7 Body camber effect on wing lift characteristics (wing tip set with most twist, $M_d = 0.80$).

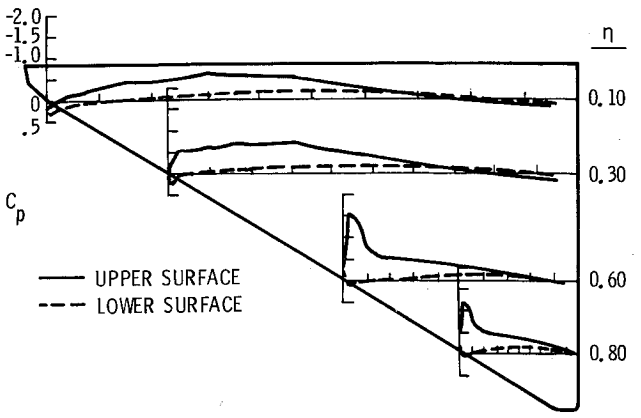

Fig. 8 Experimental pressure distribution for $B_2 + T_3$, $C_{L,d} = 0.25$, $M_d = 0.80$, and $\alpha = 6.80$ deg.

actual exterior geometry of the thick delta wing with flat surface panels. The VLM-SA code represented the configuration by modeling the camber with the slopes of its mean surface. On a wing having a round leading edge the VLM-SA code models the aerodynamic effect of leading-edge separation by the method of Kulfan.[6] (Reference 7 presents sectional normal force and pitching moment characteristics based on zero suction in order to ascertain the onset of vortical flow. Since that is not the purpose here, the leading-edge suction is allowed to be contributed to global forces and moments both before and after vortex flow onset.)

A computer representation based on the measured coordinates of the selected wing configuration is shown in Fig. 11. Comparison of this figure with Fig. 2 shows that the essential features of the wind-tunnel model have been represented. These measured coordinate data were the input for the numerical calculations; note that the sting shroud modeling was not included in the theoretical calculations. Subsequent studies, employing the PAN AIR code, showed that modeling the sting shroud did not alter the inboard C_p values over the first 50% of the chord and, hence, did not invalidate the solutions to be presented.

Force

The wing longitudinal aerodynamic characteristic predictions given by the various codes are presented in Fig. 12. The overall predictions given by the VLM-SA solutions are generally in good agreement with the data. The pitching moment results show greater stability than the experimental data and the drag-due-to-lift coefficient ΔC_D and the lift-curve slope results compare well with the experimental data near $C_{L,d}$. The $C_{D,\min}$ values employed to obtain drag-due-to-lift coefficient are 0.0063 from VLM-SA and 0.0091 from experiment. The $C_{D,\min}$ values for PAN AIR, FLO-28, and FLO-57 were not available, so the value from VLM-SA was used in the ΔC_D computation.

The PAN AIR results for lift and pitching moment correlate well with the experimental data. However, the drag-due-to-lift only correlates well near the design condition and, at higher values of the angle of attack, the measured ΔC_D is underpredicted. The FLO-28 lift coefficient estimates do not correlate well with the experimental data. It can be seen from Fig. 12 that the theory underpredicted the experiment at both angles of attack and the disagreement increases with the angle of attack. In turn, this resulted in spurious agreement for both the drag-due-to-lift and pitching moment estimates. The FLO-57 lift coefficient and drag-due-to-lift coefficient predictions are very close to the experimental values near $C_{L,d}$, but become progressively worse as C_L increases. The computed pitching moment coefficients show a greater nose-down moment than the experimental data for increasing C_L, which indicates that the computed load distribution generates a large lift contribution from behind the wing $\bar{c}/4$ than is measured.

For the experimental data, the PAN AIR solutions appear to be the better predictor of the experimental C_L, whereas the VLM-SA solutions show better agreement, up to moderate values of C_L away from $C_{L,d}$, with the drag-due-to-lift data. Note that although the VLM-SA is based on linear theory and is generally reliable for thickness ratio less than 10%, the predictions here are seen to be appropriate for the present configuration even with the values of thickness ratio being higher inboard. Possible causes for the disagreements between the various methods may be attributable to any one or all of the following: mesh density, number of iterations executed, and unmodeled flow phenomena.

Pressure

Theoretical and experimental pressure distributions at two selected stations, $\eta = 0.10$ and 0.60, for $\alpha = 6.08$ deg are presented in Fig. 13. Overall, these inviscid solutions show good agreement with the experimental lower-surface and most of the upper-surface pressure data. Note that all three codes correctly predicted the crossing of the inboard upper- and lower-surface pressures; however, the codes underpredicted the magnitude of the suction peak at both span stations presented. Nevertheless, the PAN AIR results yielded the best upper surface pressure agreement at the inboard station, while the FLO-57 predictions agreed better outboard. It is interesting to note that the outboard measured data do not exhibit the smooth onflow "design" condition since they are large negative C_p values. The predicted magnitude of the FLO-28 upper-surface results tended to be lower than those of the other codes and is reflected in the lower total lift estimates shown previously in Fig. 12.

The agreement between theoretical and experimental results, at $\alpha = 9.7$ deg (Fig. 14), is not as good. The inboard station lower-surface pressure predictions still compared well with experiment. The upper-surface predictions only approximate the trends and fail to predict, at the midchord, the recompression inboard and high suction envelope outboard.

At $\alpha = 13$ deg (Fig. 15), little agreement was observed at both $\eta = 0.10$ and 0.60, which is not surprising since the experimental pressures indicate the presence of a recompression and flow separation at the trailing edge that were not adequately modeled in the codes. Therefore, with refined physical modeling and computational arrangements, one would hope to obtain improved correlations. It should be noted that the FLO-57 solution did show the occurrence of a shed leading-edge vortex outboard of $\eta \sim 0.60$ at this α.

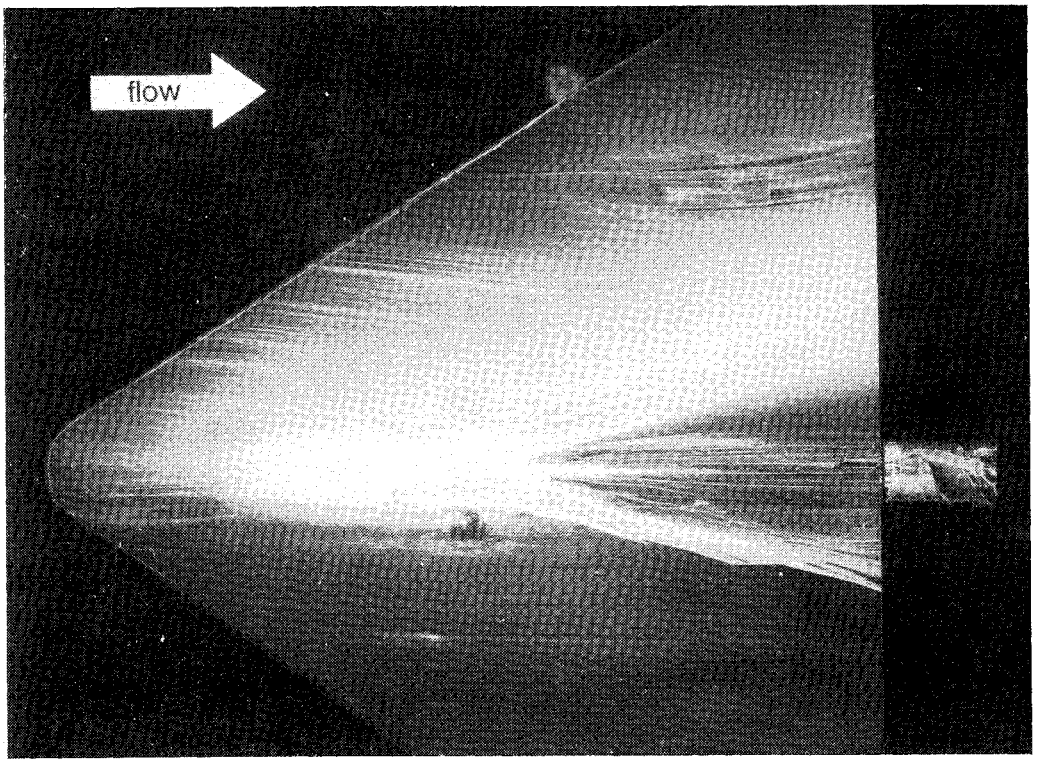

Fig. 9 Surface oil flow for $B_2 + T_3$, $\alpha = 6.07$ deg, and $M_d = 0.80$.

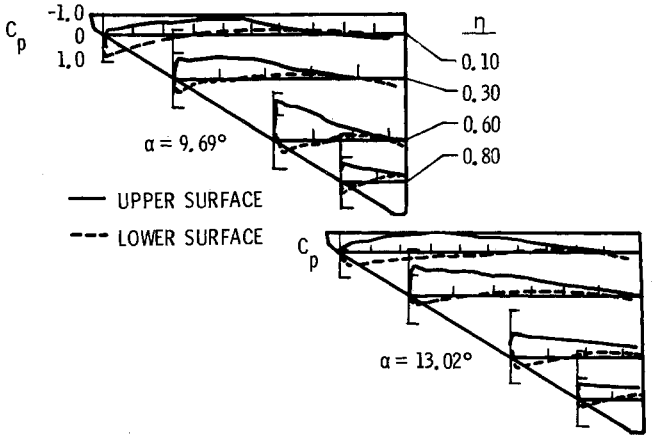

Fig. 10 Experimental pressure distributions for $B_2 + T_3$ above $C_{L,d}$ ($M_d = 0.80$).

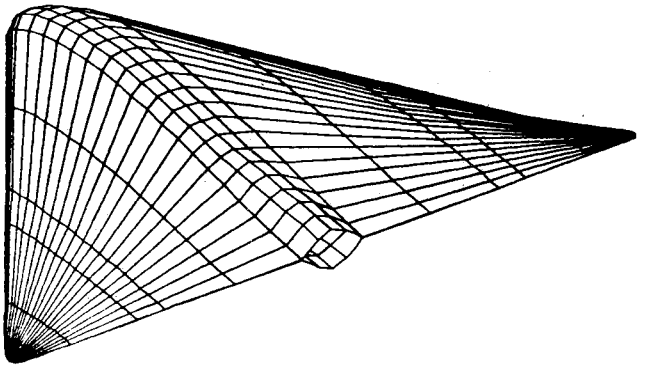

Fig. 11 Computer representation of selected wing configuration, $B_2 + T_3$.

Surprisingly, of the three codes, PAN AIR is shown to be the best overall predictor of the experimental pressure data. It should also be noted that the results plotted for this code at $\eta = 0.60$ in Figs. 14 and 15 do not show the C_p values near the leading edge, as they exceed the scale.

Conclusions

For this study, six cambered, twisted, thick delta wings were examined to determine a configuration that would satisfy the self-trimming requirement at the design lift coefficient of 0.25 and Mach number of 0.80. Analysis of the force data did not reveal a configuration satisfying the design constraints, but one was selected that came closest to the design goals and had the better overall performance. Associated experimental pressure data and limited oil-flow photograph for this wing configuration indicate that attached flow exists across the wing upper surface at the design point.

The theoretical predictions of the longitudinal aerodynamic coefficients by VLM-SA, PAN AIR, and FLO-57 agree well with the experiment near the design lift condition, except for the generally more nose-down pitching moment predicted by FLO-57. The lift solutions for the FLO-28 code underpredict the experimental data and result in spurious agreement with measured drag-due-to-lift and pitching moment data. The PAN AIR code is shown to be the better predictor of the lift coefficient and the VLM-SA shows good correlation, up to moderate value of lift coefficient, with the drag-due-to-lift estimates. The pitching moment estimates given by both codes compare well with those of the experimental data. The corresponding theoretical predictions of the pressure distributions agree well with the experiment; however, the upper-surface pressure level peaks were underpredicted. At higher angles of attack, the outboard upper-surface experimental data showed

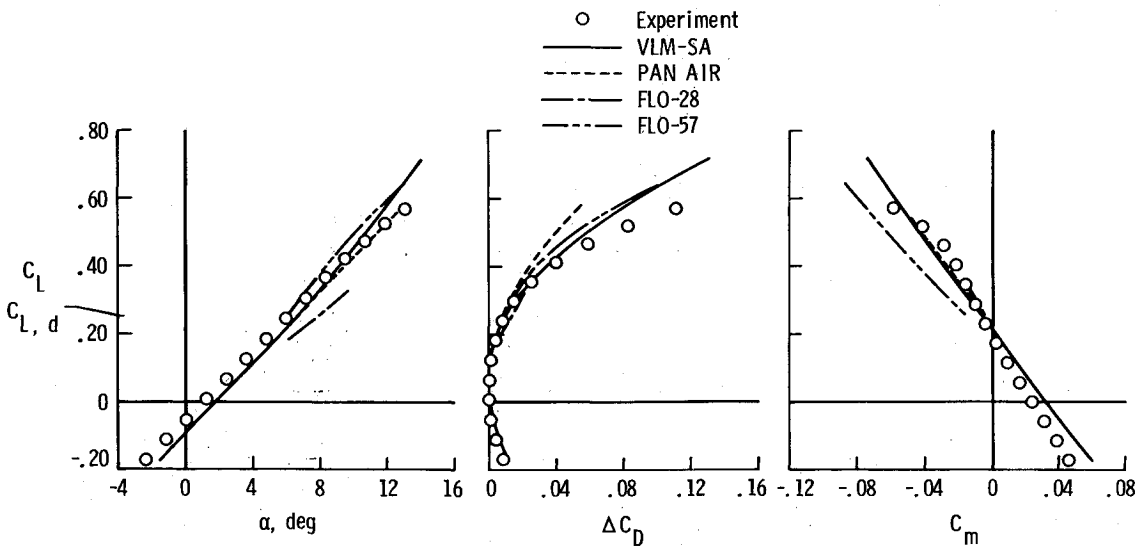

Fig. 12 Longitudinal aerodynamic characteristics for B_1+T_3 ($M_d=0.80$).

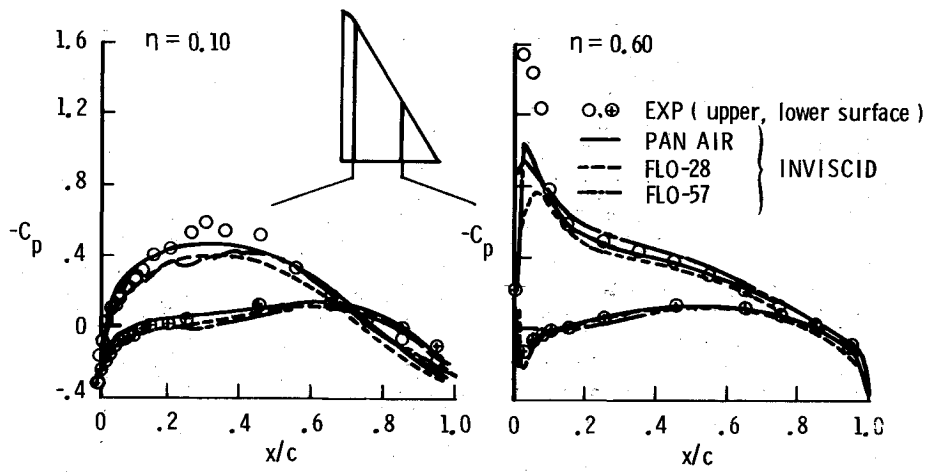

Fig. 13 Chordwise pressure distribution ($\alpha=6.08$ deg, $M_d=0.80$).

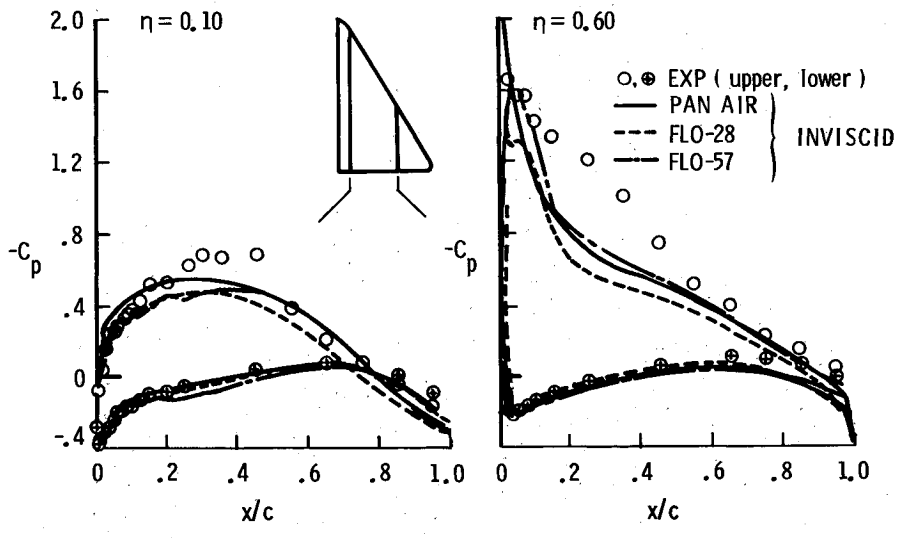

Fig. 14 Chordwise pressure distribution ($\alpha=9.70$ deg, $M_d=0.80$).

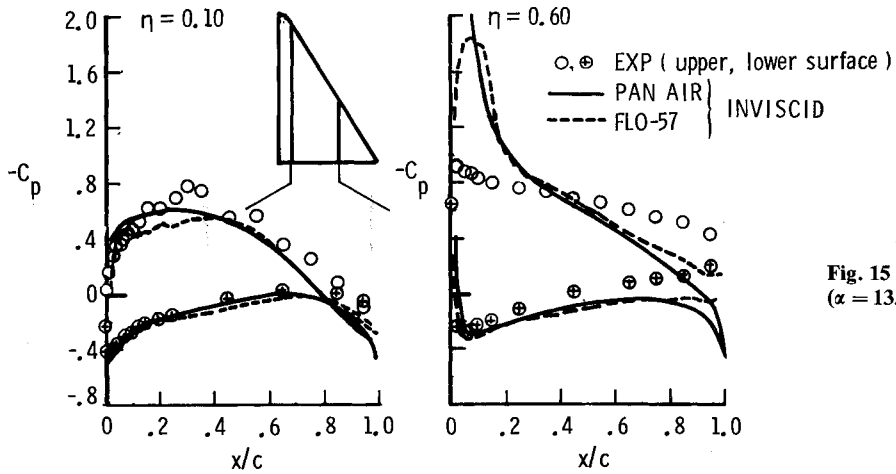

Fig. 15 Chordwise pressure distribution ($\alpha = 13.0$ deg, $M_d = 0.80$).

a reduction in the suction pressure peak value and flow separation onset; hence, the theoretical and experimental agreement was mostly limited to the lower-surface pressure values. Of the three codes capable of computing surface pressures, PAN AIR is shown to be the best overall predictor.

Acknowledgments

The FLO-57 force calculations and the FLO-28 pressure calculations were performed, respectively, by the Lockheed-California Company and the Boeing Military Aircraft Company as part of cooperative studies with NASA Langley.

References

[1]Chu, J., Lamar, J. E., and Luckring, J. M., "Longitudinal Test and Evaluation of Six 58° Cambered and Twisted Thick Delta Wings at High Subsonic Speed," NASA TM-85786, March 1985.

[2]Lamar, J. E. and Herbert, H. E., "Production Version of the Extended NASA-Langley Vortex Lattice FORTRAN Computer Program, Vol. I—User's Guide," NASA TM-83303, April 1982.

[3]Sidwell, K. W., Baruah, P. K., and Bussoletti, J. E., "PAN AIR, A Computer Program for Predicting Subsonic or Supersonic Linear Potential Flows about Arbitrary Configurations Using a Higher Order Panel Method," NASA CR-3252, May 1980.

[4]Caughey, D. A. and Jameson, A., "Finite Volume Method for Transonic Potential Flow Calculation," AIAA Paper 77-635, June 1977.

[5]Sharble, R. C. and Raj, P., "An Algebraic Grid Generation Method Coupled with an Euler Solver for Simulating Three-Dimensional Flows," AIAA Paper 83-1807, July 1983.

[6]Kulfan, R. M., "Wing Airfoil Shape Effects on the Development of Leading-Edge Vortices," AIAA Paper 79-1675, 1979.

[7]Chu, J. and Lamar, J. E., "Pressure Measurements on a Thick Cambered and Twisted 58° Delta Wing at High Subsonic Speeds," NASA TP-2713, Sept. 1987.